Single-qubit rotations in parameterized quantum circuits

S. E. Rasmussen,[1,*] N. J. S. Loft,[1] T. Bækkegaard,[1] M. Kues,[2] and N. T. Zinner[1,3,†]

[1] *Department of Physics and Astronomy, Aarhus University, DK-8000 Aarhus C, Denmark*
[2] *Hannover Center for Optical Technologies (HOT), Leibniz University Hannover, Hannover, Germany.*
[3] *Aarhus Institute of Advanced Studies, Aarhus University, DK-8000 Aarhus C, Denmark*

(Dated: November 28, 2023)

With the advent of hybrid quantum classical algorithms using parameterized quantum circuits the question of how to optimize these algorithms and circuits emerges. In this paper we show that the number of single-qubit rotations in parameterized quantum circuits can be decreased without compromising the expressibility or entangling capability of the circuit. We also compare expressibility and entangling capability across different number of qubits in parameterized quantum circuits. We also consider a parameterized photonics quantum circuit, without any single-qubit rotations, which yields an expressibility and entangling capability comparable to the best regular parameterized quantum circuits.

arXiv:2005.13548v1 [quant-ph] 27 May 2020

I. INTRODUCTION

A large-scale, fault-tolerant, universal quantum computer is one of the end goals in the quest of quantum information technology. Despite the fact that we are closer to this significant milestone than ever before, it may take years before we actually conquer this. In fact current quantum technology supports only a couple of tens of qubits and a few hundred gate operations before the noise becomes too overwhelming. Nonetheless there is growing consensus that these Noisy Intermediate-Scale Quantum (NISQ) devices may find useful application in the near future [1].

A strategy for optimizing the use of noisy quantum hardware is to divide the computational tasks between classical and quantum resources. Such a scheme is called hybrid quantum classical (HQC) algorithms. Examples of such HQC algorithms are quantum approximate optimization algorithm (QAOA) [2–4], quantum autoencoder (QAE) [5], quantum variational error corrector (QVECTOR) [6], classification via near term quantum neural networks (QNN) [7–9], quantum generative adversarial networks (qGAN) [10–13], and variational quantum eigensolver (VQE) [14–18]. Common for all these algorithms are that they share a quantum subroutine for producing parameterized trial states, where the parameters can be tuned to optimize a function value. Thus the performance of these algorithms depends on the configuration of the parameterized quantum circuits (PQC). This has led to several studies of circuit properties and capabilities [19–23]. In particular Sukin Sim *et al.* [19] has characterized the power of parameterized quantum circuits into expressibility and entangling capability.

In this article we focus on the effect of single-qubit rotations on parameterized quantum circuits. In particular we investigate whether it is possible to saturate the expressibility and entangling capability when adding more single-qubit rotations. While single-qubit rotations are often cheap to implement in the quantum circuit, they do sum up to many variational parameters for the classical optimization. The computational complexity of the classical optimization goes like $\mathcal{O}(M)$, where M is the number of single-qubit rotations. Thus reducing the number of rotations will lead to a computational speed up. So far the use of the mentioned HQC algorithms have been entirely based on rotationally saturated PQCs. This makes sense since single-qubit rotations are cheaper than entangling gate in an experimental implementation, for few qubits, when the number of qubits increases, which is necessary, e.g., if VQE is to be used on larger molecule outside the scope of classical computations. There is immediately two problems with fully saturated single-qubit rotations for PQCs consisting of many qubits: *(i)* Optimizing classical parameters is very expensive and time consuming when the number of parameters increases, *(ii)* redundant parameters increases the risk of the optimization algorithm getting stuck. We therefore pose the question: How many rotations are necessary in order to run these algorithms? This is the focus of Section II.

We also consider how the expressibility and entangling capability are affected when the number of qubits in the parameterized quantum circuit is increased up to ten qubits, where previous investigations have only considered 4 qubits [19]. In particular we consider how different entangling gates perform when the number of qubits is increased, in Section III.

Finally we present a parameterized photonics quantum circuit with a high expressibility and an asymptotic entangling capability towards unity, with just one layer and no single-qubit rotations. This can be found in Section IV. In Section V we present a summary and outlook for future work.

II. SINGLE-QUBIT ROTATIONS

In the VQE framework the quality of the results depends on how well a parameterized quantum circuit, represented by a parameter-dependent unitary matrix, $\hat{U}(\boldsymbol{\theta})$,

* stig@phys.au.dk
† zinner@phys.au.dk

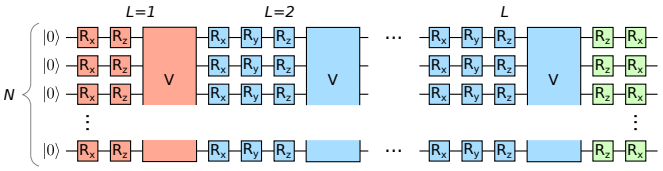


Figure 1. General implementation of a parameterized quantum circuit (PQC). Single-qubit rotations are denoted R_x, R_y, and R_z, while the multi-qubit block indicates multi-qubit operations. The initial layer (red) consists of two single-qubit rotations on each qubit and a multi-qubit gate, the bulk layers (blue) consists of three single-qubit rotations on each qubit and a multi-qubit gate, while the final part of the circuit consists of two single-qubit rotations on each qubit.

can map an initial state of N qubits $|0\cdots0\rangle$, to the ground state of a Hamiltonian $\hat{H}$. This is equivalent to optimizing $\boldsymbol{\theta}$ such that the expectation value of the Hamiltonian,

$$E(\boldsymbol{\theta}) = \langle 0\cdots0|\hat{U}(\boldsymbol{\theta})^\dagger \hat{H}\hat{U}(\boldsymbol{\theta})|0\cdots0\rangle, \tag{1}$$

is minimized. The parameters, $\boldsymbol{\theta}$, of the circuit are usually related to single-qubit rotations. Consider the PQC in Fig. 1, it consist of N qubits and L layers, where each layer implements a general rotation on the Bloch sphere, consisting of three individual rotations, one around each dimension, and a multi-qubit gate V, allowing to entangle the qubits. Since each qubit is initialized in the $|0\rangle$ state, any initial rotation about the z-axis is irrelevant, and an arbitrary Bloch rotation in the first layer (red) can be parameterized with two single-qubit gates. For the bulk layers (blue) we need three rotation gates on each qubit. In many quantum algorithms, one measures each qubit in the z-basis which by the same assumption makes final z-rotations irrelevant. However, in VQE the computation is finalized by measuring expectation values of Pauli operators, in which case all degrees of freedom matter for the qubit. Nevertheless, here we take the final rotations of the circuit (green) as a z- and x-rotation. Notice that the green gates are not considered a part of any layer and that the number of layers is equal to the number of V operations. For now we assume that the entangling gates, V, have no variational parameters, meaning that the total number of parameters is equal to the number of single-qubit rotations, which can be expressed as

$$M = N(3L+1), \tag{2}$$

where L is the number of layers and N the number of qubits For a VQE problem of fixed V, L, and N, we wish to study the effect of the number of rotations.

We wish to investigate the quality of the PQC as a function of the number of single-qubit rotations, $m \in [0, M]$, however, as this will leave 2^M possible configurations for each circuit, we take a stochastic approach. For a given number of single-qubit rotations, m, we pick a random circuit configuration producing m variational parameters. This is equivalent to fixing $M-m$ rotation angles in Fig. 1 to zero. An example circuit with $L=1$, $N=4$ and $m=6$ is shown in Fig. 2. Producing many randomly chosen circuit configurations with m rotations allow us to collect statistics about circuits with a certain 'rotations filling degree'.

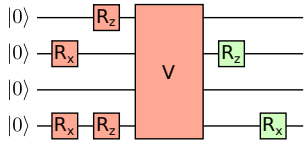


Figure 2. Example circuit with $N=4$ qubits, $L=1$ layer, and $m=6$ randomly configured single-qubit rotations.

A. Expressibility

We wish to measure and compare how well a PQC perform in a HQC algorithm, such as VQE. Currently the best way to do this is to calculate the expressibility (and entangling capability as presented in Section II B) [19]. The expressibility is a general measure of PQC, which measures how uniformly the initial state $|0\ldots0\rangle$ is mapped for random circuit parameters into the overall Hilbert space. This is done by comparing the probability distribution of the PQC with the probability of a uniform distribution in Hilbert space, i.e, an ensemple of Haar random state. In other words the expressibility states how many states the PQC can approximate.

We calculate the expressibility following the approach in Ref. [19]:

1. Pick the gate operation, V, qubit number, N, and number of layers, L.

2. For a given number of rotations, m, pick a random PQC resulting in a parameterized unitary, $\hat{U}(\boldsymbol{\theta})$.

3. Calculate expressibility of the circuit:

   (a) Uniformly sample $1000(N+1)$ sets of parameter vectors, $\boldsymbol{\theta}_1, \boldsymbol{\theta}_2$, i.e., 5000 samples for 4 qubits and 7000 samples for 6 qubits ect.

   (b) Compute the overlap fidelity of the final states, $F = |\langle 0\ldots0|\hat{U}^\dagger(\boldsymbol{\theta}_2)\hat{U}(\boldsymbol{\theta}_1)|0\ldots0\rangle|^2$.

   (c) Create a histogram over the fidelities, which we use to estimate the probability distribution, $P(F)$, of the fidelities found in the previous step. Not that this estimation will depend on the number of bins in the histogram, n_{bins}. For the sake of consistency we set $n_{\text{bins}} = 75$ as in Ref. [19]. However, note that the number of bins should be increased with increasing number of qubits.

   (d) Compare $P(F)$ with the probability distribution achieved from an ensemble of Haar random states, $P_{\text{Haar}}(F) = (2^N-1)(1-F)^{2^N-2}$, using the same number of bins as in the previous step.

We do this by computing the Kullback-Liebler divergence

$$\begin{aligned}\text{Expr} =& D_{KL}(P(F)||P_{\text{Haar}}(F)) \\ =& \sum_F P(F) \ln\left(\frac{P(F)}{P_{\text{Haar}}(F)}\right),\end{aligned} \tag{3}$$

where the sum is taken over the bins. This measure is known as the expressibility of a PQC.

4. Calculate the relative expressibility

$$\mathcal{E} = -\ln\left[\frac{\text{Expr}}{\text{Expr(Idle circuit)}}\right]. \tag{4}$$

Note that for the most expressible circuit that reaches all final states uniformly, that is $P(F) = P_{\text{Haar}}(F)$, the expressibility is 0. On the other hand, the least expressible circuit (the idle circuit with no gates) the expressibility takes a large positive value. In this case we have $\text{Expr(Idle circuit)} = (2^N - 1)\ln(n_{\text{bins}})$, which also illustrates the high dependence on the arbitrarily chosen number of histogram bins. We will therefore normalize our results with the expressibility of the idle circuit. To better resolve the results for the most expressible circuits ($\text{Expr} \sim 0$), we take the logarithm and multiply by minus one in order to make the result positive. We call this the relative expressibility, see Eq. (4).

Instead of calculating the expressibility via the Haar measure we could also have used other metrics, such as the qBAS score, where the probability distribution $P(F)$ is compared to the bars and stripes data set [24].

Had we instead tried to minimize the expressibility, this could be considered training the circuit for approximating a given probability distribution. This unsupervised machine learning task is also known as generative modeling. Such a training model is an example of data-driven quantum circuit learning (DDQCL) [24].

For each m we sample 100 random circuits and calculate their expressibility by sampling the parameters of the circuit as described in the steps above. In Fig. 3 we have plotted a 2-dimensional histogram of the expressibility as a function of the number of rotations, m, in the circuit. The calculations are done with $N = 4$ qubits in $L = 3$ layers, allowing for a maximum of $M = 40$ single-qubit rotations according to Eq. (2). The calculation is done for different entangling operations V, displayed as the inset in each subplot.

For the results of calculations with layers, i.e., $L = 1, 2,$ and 3 consult Figs. 7, 9 and 11 in Appendix B, where we also present the result of calculations for 6 and 8 qubits, Figs. 13 and 15 to 17 and Figs. 18 to 20 respectively. In each figure we consider different multi-qubit gates, V, in between the layers of rotation.

Before discussing the details of each of the different Vs we first consider some general features of the results. First of all of the plots show a 'stripe' pattern especially for low expressibility. This indicates that different groups of circuits can explore different regimes of the Hilbert space, and the addition of certain rotation gates allows the circuit to jump to different 'islands' in the Hilbert space. Another common feature is that for 8 qubits all circuit converge towards the same point. This is due to the choice of n_{bins}. When increasing the number of qubits the probability distribution of the Haar random states becomes more centered around zero. This means that for a fixed number of bins in the histogram, the first bin will dominate. This decreases the resolution of the expressibility. This could be fixed by increasing the number of bins when the number of qubits are increased. In the present paper we do not change the number of bins, as we want to compare systems with a different number of qubits. See Section III.

$V =$ IDENTITY In Fig. 3(a) we consider the case of no multi-qubit gate, i.e. the identity (note that the single-qubit rotations are still present; it is V which is the identity, not the PQC). As we do not expect this to return a large expressibility, we do this in order to be able to compare the remaining multi-qubit gates to this. We see that the the expressibility converges towards a relative expressibility of $\mathcal{E} = 6$. We see that it has already converged for 25 single-qubit rotations, meaning that applying any more rotations does not improve the circuit's expressibility. For less layers, we of course observe the same tendency (for one layer we do not saturate the expressibility, as we cannot add enough rotations). If we increase the amount of qubits we also observe that we saturate the expressibility with single rotations. For $N = 6$ qubits (see Fig. 17(a)) the relative expressibility converges at $\mathcal{E} = 7$, and is converged around 30 rotations. For 8 qubits we observe the same behavior, i.e., the expressibility saturates. This time it converges towards $\mathcal{E} = 7.5$ and convergence is reached for around 30 rotations (see Fig. 19(a)).

$V =$ CNOTs One of the most frequently used entangling two-qubit gates is the CNOT gate. We therefore consider the case where V is a CNOT between each qubit. See Fig. 3(b) for the case of 4 qubits and 4 layers. Once again the relative expressibility converges within 30 single-qubit rotations, however, this time the relative expressibility goes towards $\mathcal{E} = 10$. Thus the change of entangling gate increases the expressibility significantly, as expected. For less layers the story is the same; the expressibility is saturated for more than 30 single-qubit rotations. This means that for one and two layers we do not saturate the expressibility, as we have less than 30 rotations in both cases. However, any more than three layers of CNOTs and 30 single-qubit rotations seems to be a waste of resources as the expressibility does not increase beyond this. For $N = 6$ qubits (see Figs. 13 and 15 to 17(b)) we observe the same tendency, however, the relative expressibility converges towards $\mathcal{E} = 9$. This happens at around 40 single-qubit rotations, which can be obtained for just two layers. Turning towards the case of 8 qubits we again observe a saturation of the expressibility (see Fig. 19(b)).

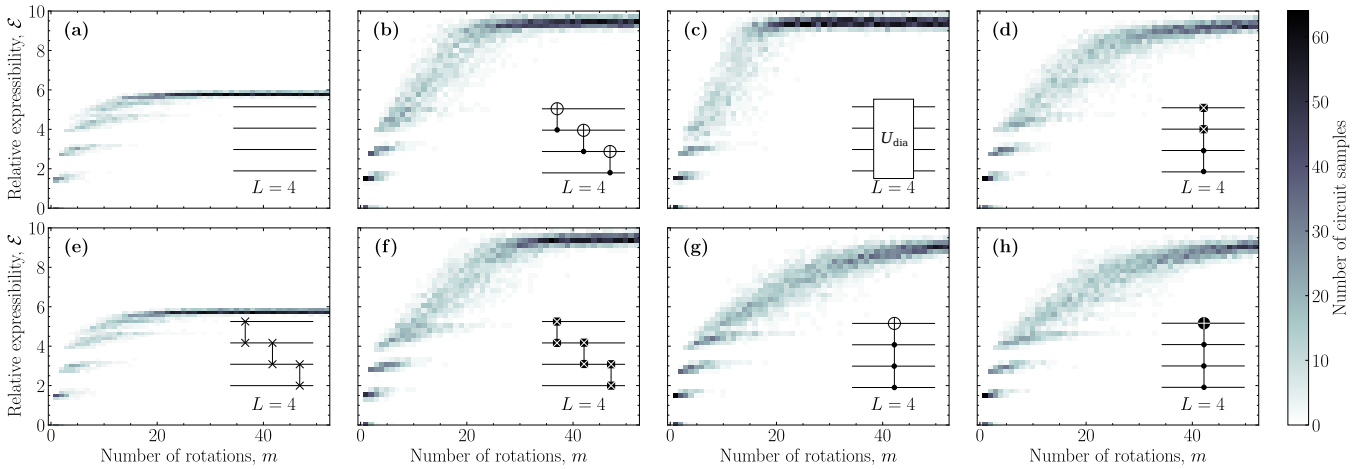


Figure 3. Relative expressibility of different circuits with $N = 4$ qubits and $L = 3$ layers as a function of the number of rotations. The inset in the right upper corner of each plot shows the entangling gate used in each layer. **(a)** Identity, **(b)** three CNOTs, **(c)** diamond gate, **(d)** double controlled iSWAP, **(e)** three SWAPs, **(f)** three iSWAPs, **(g)** triple controlled NOT, **(h)** triple controlled iNOT.

Convergence is reached after approximately 30 single-qubit rotations at a relative expressibility $\mathcal{E} = 7.5$, lower than for both 4 and 6 qubits, and the same as for no entangling V gate (see Fig. 19(a)).

$V =$ SWAPs Another frequently used two-qubit gate is the SWAP gate. We therefore consider the case where V is a SWAP between each qubit. See Fig. 3(e) for the case of 4 qubits and 4 layers. We see that this configuration behaves identically to the identity in subfigures (a). This is the case for all combinations of layers, L, and qubits, N. This may not be surprising as the SWAP gate is not an entangling gate, with a two-qubit entangling power of zero [25].

$V = i$SWAPs An entangling version of the SWAP gate is the iSWAP gate. The iSWAP gate has an entangling power equivalent to the CNOT gate, and occurs naturally in systems with XY-interaction or Heisenberg models, such as solid state systems [26, 27], superconducting circuits [28], and in cavity mediated between spin qubits and superconducting qubits [29–31]. In Fig. 3(f) we present the relative expressibility where the V gate is an iSWAP gate between each qubit. The relative expressibility of this configuration goes towards the same as for the CNOT, however, it converges a bit slower. For 4 qubits the difference is about 5 rotations, however, for 6 qubits it is more obvious with a difference of around 20 single-qubit rotations (compare Fig. 17(b) and (f)). The behavior for 8 qubits and the iSWAP gates is the same as for the other 8 qubit PQC.

$V =$ DIAMOND An example of an entangling 4-qubit gate is the Diamond gate [32], which is an entangling swapping gate with two controls, which must be in an entangling state in order to control the swapping operation. Contrary to the two-qubit gates mentioned above the Diamond gate cannot be nicely synthesized by one- and two-qubit gates. It does, however, naturally occur in superconducting circuit schemes for quantum information processing. See Appendix A for more details. due to the fact that the Diamond gate is a highly entangling four-qubit gate we expect that it will show a larger expressibility.

In Fig. 3(c) we present the the expressibility for circuits with 4 qubits, 4 layers and $V = U_{\text{dia}}$, where U_{dia} is the Diamond gate. We see that the expressibility converges rapidly towards $\mathcal{E} = 10$, which it reaches within 20 single-qubit rotations, which is less than for both the CNOT and iSWAP gates in subfigures (b) and (f). We observe the same behavior for 6 qubits (Figs. 13 and 15 to 17(c)); when the Diamond gate is used as an entangling gate, convergence is reached faster than for the CNOT and iSWAP gates. For 8 qubits the performance of the Diamond gate is reduced to the same as the other gates, see Figs. 19 and 20.

$V =$ MULTI-QUBIT GATES One might wonder if this means that multi-qubit gates are superior to two-qubit entangling gates? We therefore consider a few other multi-qubit gates. A well known three-qubit gate is the Toffoli gate, a NOT gate with two control qubits, [33] due to the fact that it, together with the Hadamard gate constitutes a universal set of quantum gates [34]. The Toffoli gate can straightforwardly be expanded to an n-controlled NOT gate [35–38]. Another version of the n-controlled NOT gate is the n-controlled iNOT gate, which is a controlled NOT gate which obtains a phase of i if the NOT gate is activated. The n-controlled NOT gate can readily be implemented in systems where this phase occur natively, such as superconducting circuits [39]. Related to the Toffoli gate is the Fredkin gate [40], a controlled SWAP gate. The Fredkin gate can also be expanded to a SWAP gate with multiple controls. Due to the fact that the Fredkin gate itself is difficult to implement we consider instead a multiple controlled iSWAP gate, as it occurs

naturally in many solid state system used to implemented quantum information schemes [41–43].

We consider the n-bit iToffoli, n-bit Toffoli, and the n-bit iSWAP gate as the V gate one at a time. The result of calculations with these gates can be seen in subfigures (d), (g), and (h) of Fig. 3, respectively, and in the same subfigures in Appendix B. Common for all three gates are that they converge towards the same relative expressibility as the other entangling gates, namely $\mathcal{E} = 10$ for 4 qubits. However, they are much more depended on the number of rotations, as the convergence point is only reached for the maximum amount of rotations. The main difference of the three gates is that the double controlled iSWAP in Fig. 3(h) converges a bit faster than the multiple controlled NOT gates. This is however, not something which can be seen for 6 qubits (see Appendix B Fig. 17), where all three multi-qubit gates converge at the same rate. Thus the faster conversion of the double controlled iSWAP is probably due to the fact that it has twice as many target qubits compared to the multiple controlled NOT gates, something which is less significant for more qubits. An interesting thing to notice is the fact that the Diamond gate seems to converge much faster than the double controlled iSWAP gate (compare subfigure (c) to (d)). This is despite the fact that both gates are swapping gates with two controls. This is probably due to the fact that the controlling part of the Diamond gate requires a superposition state in order to activate the swap, compared to the multiple controlled iSWAP gate which does not require a superposition. For 6 qubits (see Appendix B Fig. 17) we also observe that the three multi-qubit gates just barely outperform the non-entangling gates in Fig. 17(a) and (b). This could be due to the fact that most of the qubits become control qubits when the number of qubits increases, leaving the gate performing identity operations on most states.

Table I shows an overview of the saturation points of the different gates discussed above. We note that there may be other entangling gates which outperform the gates we have considered here.

Table I. Overview of saturation point, given in number of single-qubit rotations, m, and number of layers, L, for the different multi-qubit gates considered in this sections. The corresponding expressibility and entangling capability is also show when applicable.

	$N=4$				$N=6$			$N=8$		
Gate	m	L	Expr	Ent	m	L	Expr	m	L	Expr
Identity	25	2	6	-	30	2	7	35	2	7.5
CNOTs	30	3	10	0.8	40	3	9	35	2	7.5
iSWAPs	35	3	10	0.8	60	3	9	40	2	7.5
Diamond	20	2	10	0.8	30	2	9	30	2	7.5
Multi-qubit	48	4	10	0.6	40	3	7.5	40	2	7.5

B. Entangling capability

One of the advantages of HQC algorithms over classical algorithms is their potential ability to generate entangled states. Therefore we also wish to measure how well quantum circuits can produce entangled states. Reference [19] proposes to use the entangling capability to measure this and defines it as the average Meyer-Wallach entanglement measure [44], where the average is taken over a uniformly sampled set of parameters $\boldsymbol{\theta}$. The entangling capability then lies between zero and one with zero being a none-entangling circuit and one representing a maximally entangling circuit. We wish to investigate whether the entangling capability saturates around the same amount of single-qubit rotations as the expressibility saturates.

We calculate the entangling capability for the same circuits for which we calculated the expressibility. However, we only consider the circuits with entangling multi-qubit gates, i.e., not the identity and SWAP-gates. We expect that the entangling capability is saturated around the same point as the expressibility is saturated, in which case we can conclude that the PQC is indeed saturated. We present 2-dimensional histograms of the entangling capabilities in Fig. 4, for the case of $N = 4$ qubits and $L = 3$ layers. For the result of $L = 1, 2$, and 3 layers consult Figs. 8, 10 and 12 in Appendix B.

V = CNOTs and V = iSWAPs From Fig. 4(a) we observe that the entangling capability of the case where we have a CNOT gate between each qubit saturates at around 0.8 at approximately 30 single-qubit rotations, which is the same as for the expressibility. In the case of the iSWAP gate, in Fig. 4(d) we see that the entangling capability saturates a bit below 0.8 and the saturation point is later than for the CNOT gates. This is comparable to the expressibility calculation, where the iSWAP gates also performed lightly worse than the CNOT gates.

V = Diamond The Diamond gate in Fig. 4(b) also saturates at around 0.8, however, in terms of the number of single-qubit rotations it out-performs the other gates having almost saturated already at 20 single-qubit rotations. This is also comparable to the expressibility calculation, where the Diamond gate also saturated at around 20 single-qubit rotations.

V = Multi-qubit gates Finally the three gates with multiple control perform only averagely with a maximal entangling capability of 0.5, see Fig. 4(c), (e), and (f). Equivalently to the expressibility we need the maximum number of rotations for the entangling capabilities to reach maximum.

We conclude that the entangling capability and expressibility saturate for the same number of qubit rotations. Due to the computational complexity, we only sample entangling capability for 6 or 8 qubits. However, we do expect the same results as in the 4 qubits case. In the following section we do, nonetheless, consider the entangling capability and the expressibility as the number of qubits increases.

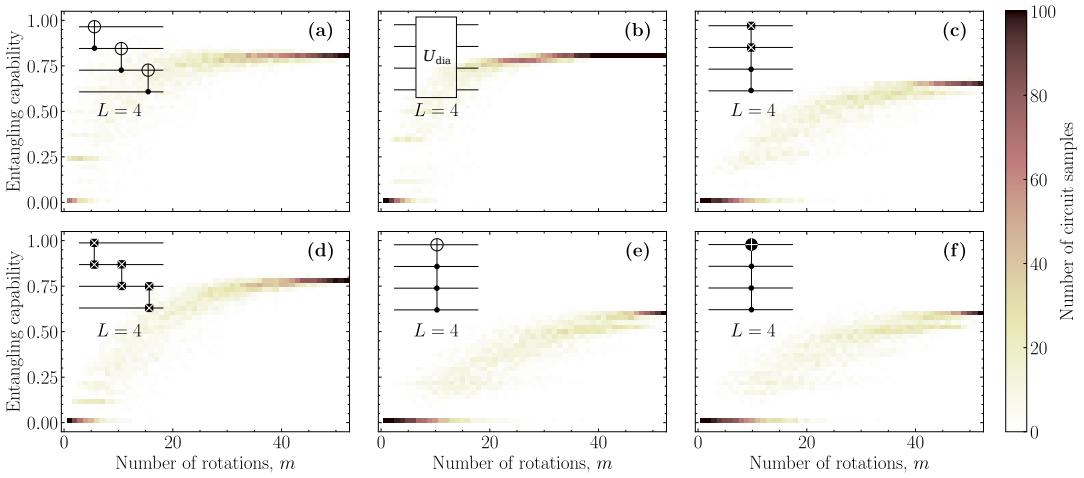


Figure 4. *Entangling capability* of different circuits with $N = 4$ qubits and $L = 3$ layer as a function of the number of rotations. The inset in the right upper corner of each plot shows the entangling gate used in each layer. **(a)** three CNOTs, **(b)** diamond gate, **(c)** double controlled *i*SWAP, **(d)** three *i*SWAPs, **(e)** triple controlled NOT, **(f)** triple controlled *i*NOT.

III. INCREASING THE NUMBER OF QUBITS

In the light of the fact that all 8 qubit PQC seems to converge approximately towards the same relative expressibility, we investigate the relative expressibility as a function of the number of qubits. We therefore plot the relative expressibility for different V gates in the top part of Fig. 5. We plot for up to three layers and in order to ensure that the expressibility has converged in relation to the number of single-qubit rotations we use the maximum number of rotations, i.e., M rotations. We use a selection of the same gates discussed in the previous section: The identity, CNOT's, the Diamond gate, the multi-qubit controlled NOT gate, and a photonics gate which is discussed in more detail in Section IV.

For less than 8 qubits we observe that the relative expressibility is quite scattered, with the entangling gates yielding the best expressibility, and the identity gate yielding worst expressibility. However, as the number of qubits increases the relative expressibility seems to converge towards $\mathcal{E} = 6.5$ for all cases. This is due to the fact that when the number of qubits increases the Haar measure dominate at low fidelity meaning that the lowest bins dominates in the calculation of the expressibility. When the number of qubit becomes sufficiently large only the lowest bin becomes relevant when calculating the expressibility. One should therefore consider increasing the number of bins if one wishes to investigate the expressibility for more qubits. However in order to compare the expressibility for circuits of a different number of qubits one should have the same number of bins, which is why we have chosen bins = 75 for all calculations. This also mean that even though the expressibility seems to converge towards a lower value for larger N it does not necessarily mean these PQCs are worst than similar PQC for lower N. It is simply a result of the way the expressibility is defined. One should be cautious when comparing across different number of qubits.

Contrary to the expressibility the entangling capability is not depended on any number of qubits dependent parameter, and we does not expect it to converge towards a specific value for all cases. We plot the entangling capability in the bottom part of Fig. 5. Without any entangling gates the entangling capability is of course zero. When we introduce the CNOT gates we obtain an asymptotically increasing entangling capability. Not surprisingly we see that more layers increase the entangling capability of the CNOT gates. We observe that for up to three layers it does not look like the entangling capability converge towards one, but rather towards 0.7 for one layer, 0.92 for two layers, and 0.95 for three layers. However, this could be fixed simply by adding more layers, in which case it converges towards one.

The entangling capability of *i*SWAP gates between each qubit is constant for a single layer around 0.3, which is significantly lower than for the CNOT gates, despite these both having the maximum entangling power [25]. However, increasing the number of layers greatly increases the entangling capability of the circuit, however, it still remains inferior to a circuit with CNOT gate for the same amount of layers.

Turning to the Diamond gate we see that for one layer its entangling capability is approximately equal to that of the CNOT gates, though it does seem to increase a bit slower than the CNOT gate. However, for two layers it outperforms the CNOT gates for three layers. For three layers of the Diamond gate it looks like the entangling capability converges towards one.

Contrary to the other entangling gates the entangling capability of the multi-qubit controlled NOT gate converges towards zero as the number of qubits increases. This is probably due to the fact that for a large number of control qubits the multi-qubit gate resembles the identity

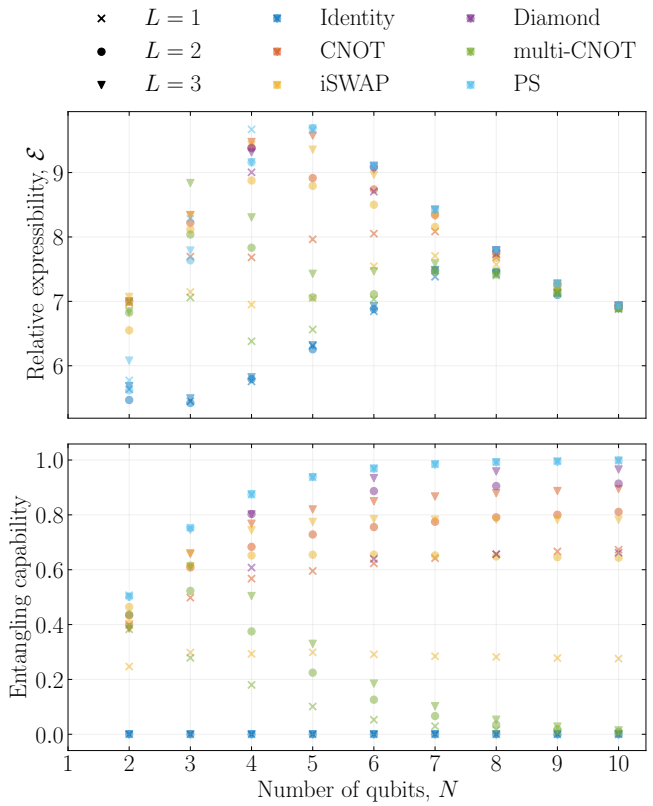


Figure 5. *Top:* Relative expressibility and *bottom:* entangling capability for different circuit configurations as a function of the number of qubits. Dark blue colored markers indicates that no entangling gate is used, i.e., $V = I$. Red markers indicate that CNOT gates are used as entangling gate, equivalently to the inset in e.g. Fig. 3(b). Yellow markers indicate that iSWAP gates are used as entangling gates, equivalently to the inset in e.g. Fig. 3(c). Purple markers indicate Diamond gates are used as entangling gates, equivalently to the inset in e.g. Fig. 19(e). Green markers indicate that the multi-qubit controlled NOT gate is used as an entangling gate equivalently to the inset in Fig. 3(g). Light blue markers indicates a photonics frequency comb system circuit consisting of a single phase shaper gate. Note that the frequency comb system consists of one qudit with 2^N state, where N is the number of qubits in the other PQCs. See Section IV for details. Crosses indicates one layer circuit, circles indicates two layers and triangles indicates three layers. In order to ensure convergence all circuits are simulated with with the maximum number of rotations, i.e., M rotations, with the exception of the photonics circuit which have zero single-qubit rotations.

quite well.

IV. PHOTONIC PARAMETERIZED QUANTUM CIRCUITS

Is it possible to create powerful parameterized quantum circuits completely without single-qubit rotations capable of performing HQC algorithms? This might be useful if

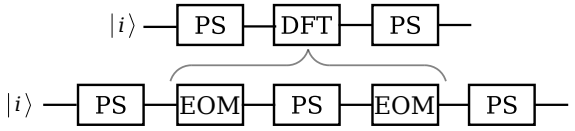


Figure 6. *Upper:* Photonic frequency comb qudit parameterized quantum circuit consisting of a phase shaper gate (PS) followed a discrete Fourier transform gate (DFT) followed by yet another phase shaper gate. *Lower:* The gate sequence used to realize the DFT gate consisting of a phase shaper gate sandwiched in between two electro-optic modulators. The input state, $|i\rangle$, is an even superposition, see Eq. (5).

we consider photonic systems in fiber optics, where each photon may have more than two internal states [45–50]. Such state featuring $d > 2$ internal levels are typically denoted 'qudits'. In this case it may be more favorable to apply other operations than rotations on two-level subsets.

We consider a qudit realized by a frequency comb system, i.e., where each state $|\omega\rangle$ corresponding to a photon with the given frequency. Being in a frequency comb system, all neighboring qudit states have the same frequency difference $\Delta\omega$ and the states can thus be numbered as $|n\rangle = |\omega_0 + n\Delta\omega\rangle$ with $|\omega_0\rangle$ being some offset frequency. If the qudit has 2^N levels we can easily map each qudit state to a states of the N qubits. The qubit is initialized in the even superposition state

$$|i\rangle = \frac{1}{\sqrt{d}} \sum_{n=1}^{d} |n\rangle. \tag{5}$$

We consider the single frequency comb PQC in Fig. 6, on which we act with a single gate: a phase shaper (PS) gate [51, 52].

The phase shaper gate is configured as a single Fourier transform phase shaper gate, which in principle works by separating each frequency and then independently and in parallel controlling the amplitude and phase of each frequency component. However, since amplitude modulation (attenuation) only reduces the total population, we will only be using it for controlling the phases of each frequency. As stated, this can be done in parallel and independently, thus we can write the corresponding gate operator as

$$\hat{U}_{\text{PS}} = \sum_{j=1}^{d} e^{i\theta_j} |j\rangle\langle j|, \tag{6}$$

where d is the number of frequency bins in the system, which should be equal to the number of qudit levels. The phase, θ_j, of each mode is the parameter we wish to optimize in our parameterized quantum circuit. This means that there are 2^N parameters to optimize classically. Thus the number of parameters increases more rapidly than the case of regular PQCs as in Fig. 1, where the number of parameters increases linearly. This means

that we increase the complexity of the classical part of the computation, however, it significantly decreases the quantum mechanical complexity of the calculation as we are now only concerned with a few gates per layer.

We calculate the expressibility and entangling capability of the phase shaper gate acting on the state in Eq. (5), i.e., $\hat{U}_{\rm PS}|i\rangle$, for a different number of qudit levels. In order to relate this to the other qubit circuits we consider 2^N levels and plot the results in Fig. 5 together with qubit PQCs with N qubits. We observe that the relative expressibility of the phase shaper PQC matches the expressibility of the best qubit PQCs.

We also note that the entangling capability of the phase shaper gate beats all of the regular PQCs even for just a single layer. This fact means that we can significantly decrease the quantum mechanical part of the computation as we only require one gate in our circuit in order to obtain optimal expressibility and entangling capability. This is, however, at the expense of increasing number of parameters. A priori, one might consider employing the same trick as with the single rotations in qubit PQC, in Section II, and remove some of the phase rotations in the phase shaper gate. However, this is not a fruitful tactic. A simulation of the expressibility of the phase shaper gate as a function of the number of phase rotations, shows that gate needs more or less all phase rotations for it to have a significant expressibility. See Fig. 21 in the appendix for plots of the result. We have only considered systems consisting of a single qudit, however, it would be interesting to see if one could find some middle ground between one 2^N-level qudit and N qubits, where the number of parameters is optimal without increasing the quantum mechanical complexity too much.

Note that the entangling capability only makes sense in relation to the phase shaper circuit as long as we apply a 1:1 mapping between the qudit states and the qubit states.

Despite the superior expressibility and entangling capability of the phase shaper gate, it is still not evident that it can be used in HQC algorithms such as the variational quantum eigensolver and others. If we consider the resulting state when acting with the phase shaper on the state in Eq. (5) we find

$$\hat{U}_{\rm PS}|i\rangle = \frac{1}{\sqrt{d}}\sum_{j=1}^{d} e^{i\theta_j}|j\rangle. \tag{7}$$

Thus we have obtained an even superposition with full control over the phases. However, it is not possible to remove any states from the superposition by varying the parameters. This could become a significant problem if the states are used for HQC algorithms. It is possible to vary the amplitudes of the PS gate at the expense of decreasing the possibility of observing the photon. However, preliminary tests indicate that variation of amplitude in the PS gate does not lead to noticeable improvement.

In order to add some entangling power to the PS gate, we propose to add a discrete Fourier transform (DFT) gate [46] followed by another phase shaper gate. The Discrete Fourier Transform gate is essentially a uniform beamsplitter which splits the beam into a number of modes, where the phase of each mode is matched to that of the a discrete Fourier transform. Such a gate can be created by combining an electro-optic phase modulator (EOM), a phase shaper, and then once more an EOM [46]. See Fig. 6.

The electro-optic phase modulator is composed of a waveguide which is formed by diffusing an electro-optic material (typically Ti) into a dielectric substrate (typically $LiNbO_3$) and a set of driving electrodes [53]. Consider the electrodes driven by a voltage function $\Delta V(t) = V_0\cos(\Delta\omega_0 t + \theta)$ plus an unimportant constant contribution, which result in a global phase change, which is why we ignore it. Classically this results in a phase shift of the incoming electromagnetic wave of $\exp(-i\pi\Delta V(t)/V_\pi)$. Here, V_π is the DC voltage required for a constant π phase shift. For simplicity we absorb the constants π and V_π into $\Delta V(t)$. The resulting quantum transformation of the electro-optic phase modulator in photon-frequency notation is then

$$\hat{U}_{\rm EOM} = \int \frac{d\omega}{2\pi}\sum_{n=-V_0-1}^{V_0+1}(-ie^{-i\theta})^n J_n(V_0)\hat{a}^\dagger(\omega+n\Delta\omega_0)\hat{a}(\omega), \tag{8}$$

where J_n are the Bessel functions of the first kind and $\hat{a}$ and $\hat{a}^\dagger$ are the photon annihilation and creation operators. Thus each EOM gate has two parameters V_0 and θ which can be controlled. Combining two EOM gate around a single phase shaper gate can be used to realize a DFT gate [46], see Fig. 6.

We expect that this combination of gates will perform well in a HQC algorithm utilizing frequency photonics systems, since it will be capable of controlling both the phase and amplitude of the states in the superposition. We leave it to future work to verify this. A calculation of the expressibility and entangling capability of the circuit yields the same result as for the single phase shaper gate, which we believe is the maximum possible expressibility and entangling capability for this number of bins.

V. CONCLUSION AND OUTLOOK

We have investigated the expressibility and entangling capability of Ref. [19] for parameterized quantum circuits for at different number of single-qubit rotations. We have found that both the expressibility and entangling capability can be saturated using less single-qubit rotations than the maximum amount. In particular it should be enough to employ 5-10 rotations per qubit. This could significantly decrease the classical computational complexity of many hybrid quantum classical algorithms. We also find that it is subordinate where these single-qubit rotations are placed in the circuit.

Once the saturation point is achieved in regards to the single-qubit rotations, the only remaining parameter

to change is multi-qubit gates in each layer. We find that when the number of qubits in the circuit exceeds nine, good expressibility can be achieved with just single-qubit rotations. However, the entangling capability is still dependent on multi-qubit gates, and thus one must use a highly entangling gate as a multi-qubit gate, such as the CNOT gate or the Diamond gate [32], which seems to converge towards an entangling capability of 1 when the number of the qubits increases. Other gates such as the iSWAP gate or multi-qubit gates dominated by controls are not as adequate.

We also find that the expressibility is dependent on the multi-qubit gate being an entangling gate. Using non-entangling gates, such as SWAP gates, in each layers yields an expressibility equal to that of the identity. This shows that the expressibility cannot be completely separated from the quantum mechanical part of PQCs.

It is our assesment that an efficient parameterized quantum circuit can be created by employing a number of highly entangling gates such as the Diamond gate or the CNOT in each layer, for three layers and then doing 5-10 single-qubit rotations on each qubit. The placement of the single-qubit rotations can be randomized.

We have also considered whether it was possible to create a useful photonic PQC, which means using no single-qubit rotations. Using a single phase shaper gate, we obtain an expressibility and an entangling capability comparable to the best regular PQCs. This could open up for a new exploitation of photonic circuits in HQC algorithms, which could increase the computational power of such algorithms, since photonics might be able to accommodate more states than the current working number of qubits in e.g. superconducting circuits.

A high expressibility and entangling capability are of course not enough to prove that PQCs are useful for HQC algorithms. A next step would then be to investigate the PQCs mentioned in this paper in an actual HQC setting.

ACKNOWLEDGMENTS

This work is supported by the Danish Council for Independent Research and the Carlsberg Foundation. The numerical results presented in this work were obtained at the Centre for Scientific Computing, Aarhus `http://phys.au.dk/forskning/cscaa/`. M.K. received support by the German Federal Ministry of Education and Research (Project PQuMAL).

[1] J. Preskill, Quantum **2**, 79 (2018).
[2] E. Farhi, J. Goldstone, and S. Gutmann, "A quantum approximate optimization algorithm," (2014), arXiv:1411.4028.
[3] J. S. Otterbach, R. Manenti, N. Alidoust, A. Bestwick, M. Block, B. Bloom, S. Caldwell, N. Didier, E. S. Fried, S. Hong, P. Karalekas, C. B. Osborn, A. Papageorge, E. C. Peterson, G. Prawiroatmodjo, N. Rubin, C. A. Ryan, D. Scarabelli, M. Scheer, E. A. Sete, P. Sivarajah, R. S. Smith, A. Staley, N. Tezak, W. J. Zeng, A. Hudson, B. R. Johnson, M. Reagor, M. P. da Silva, and C. Rigetti, "Unsupervised machine learning on a hybrid quantum computer," (2017), arXiv:1712.05771.
[4] N. Moll, P. Barkoutsos, L. S. Bishop, J. M. Chow, A. Cross, D. J. Egger, S. Filipp, A. Fuhrer, J. M. Gambetta, M. Ganzhorn, A. Kandala, A. Mezzacapo, P. Müller, W. Riess, G. Salis, J. Smolin, I. Tavernelli, and K. Temme, Quantum Science and Technology **3**, 030503 (2018).
[5] J. Romero, J. P. Olson, and A. Aspuru-Guzik, Quantum Sci. Technol. **2**, 045001 (2017).
[6] P. D. Johnson, J. Romero, J. Olson, Y. Cao, and A. Aspuru-Guzik, "Qvector: an algorithm for device-tailored quantum error correction," (2017), arXiv:1711.02249.
[7] E. Farhi and H. Neven, "Classification with quantum neural networks on near term processors," (2018), arXiv:1802.06002.
[8] V. Havlícek, A. D. Córcoles, K. Temme, A. W. Harrow, A. Kandala, J. M. Chow, and J. M. Gambetta, Nature **567**, 209 (2019).
[9] M. Schuld, A. Bocharov, K. M. Svore, and N. Wiebe, Phys. Rev. A **101**, 032308 (2020).
[10] P.-L. Dallaire-Demers and N. Killoran, Phys. Rev. A **98**, 012324 (2018).
[11] S. Lloyd and C. Weedbrook, Phys. Rev. Lett. **121**, 040502 (2018).
[12] C. Zoufal, A. Lucchi, and S. Woerner, npj Quantum Information **5**, 103 (2019).
[13] D. Zhu, N. M. Linke, M. Benedetti, K. A. Landsman, N. H. Nguyen, C. H. Alderete, A. Perdomo-Ortiz, N. Korda, A. Garfoot, C. Brecque, L. Egan, O. Perdomo, and C. Monroe, Science Advances **5** (2019), 10.1126/sciadv.aaw9918.
[14] A. Peruzzo, J. McClean, P. Shadbolt, M.-H. Yung, X.-Q. Zhou, P. J. Love, A. Aspuru-Guzik, and J. L. O'Brien, Nature Communications **5**, 4213 (2014).
[15] J. R. McClean, J. Romero, R. Babbush, and A. Aspuru-Guzik, New Journal of Physics **18**, 023023 (2016).
[16] P. J. J. O'Malley, R. Babbush, I. D. Kivlichan, J. Romero, J. R. McClean, R. Barends, J. Kelly, P. Roushan, A. Tranter, N. Ding, B. Campbell, Y. Chen, Z. Chen, B. Chiaro, A. Dunsworth, A. G. Fowler, E. Jeffrey, E. Lucero, A. Megrant, J. Y. Mutus, M. Neeley, C. Neill, C. Quintana, D. Sank, A. Vainsencher, J. Wenner, T. C. White, P. V. Coveney, P. J. Love, H. Neven, A. Aspuru-Guzik, and J. M. Martinis, Phys. Rev. X **6**, 031007 (2016).
[17] A. Kandala, A. Mezzacapo, K. Temme, M. Takita, M. Brink, J. M. Chow, and J. M. Gambetta, Nature **549**, 242 (2017).
[18] Y. Cao, J. Romero, J. P. Olson, M. Degroote, P. D. Johnson, M. Kieferová, I. D. Kivlichan, T. Menke, B. Peropadre, N. P. D. Sawaya, S. Sim, L. Veis, and A. Aspuru-Guzik, Chemical Reviews **119**, 10856 (2019).

[19] S. Sim, P. D. Johnson, and A. Aspuru-Guzik, Advanced Quantum Technologies **2**, 1900070 (2019).

[20] M. R. Geller, Phys. Rev. Applied **10**, 024052 (2018).

[21] Y. Du, M.-H. Hsieh, T. Liu, and D. Tao, "The expressive power of parameterized quantum circuits," (2018), arXiv:1810.11922.

[22] M. Benedetti, E. Lloyd, S. Sack, and M. Fiorentini, Quantum Science and Technology **4**, 043001 (2019).

[23] T. Hubregtsen, J. Pichlmeier, and K. Bertels, "Evaluation of parameterized quantum circuits: on the design, and the relation between classification accuracy, expressibility and entangling capability," (2020), arXiv:2003.09887.

[24] M. Benedetti, D. Garcia-Pintos, O. Perdomo, V. Leyton-Ortega, Y. Nam, and A. Perdomo-Ortiz, npj Quantum Information **5**, 45 (2019).

[25] C. P. Williams, *Explorations in Quantum Computing* (Springer, 2011).

[26] T. Tanamoto, K. Maruyama, Y.-x. Liu, X. Hu, and F. Nori, Phys. Rev. A **78**, 062313 (2008).

[27] T. Tanamoto, Y.-x. Liu, X. Hu, and F. Nori, Phys. Rev. Lett. **102**, 100501 (2009).

[28] A. M. Zagoskin, S. Ashhab, J. R. Johansson, and F. Nori, Phys. Rev. Lett. **97**, 077001 (2006).

[29] A. Imamoḡlu, D. D. Awschalom, G. Burkard, D. P. DiVincenzo, D. Loss, M. Sherwin, and A. Small, Phys. Rev. Lett. **83**, 4204 (1999).

[30] M. Benito, J. R. Petta, and G. Burkard, Phys. Rev. B **100**, 081412R (2019).

[31] A. Blais, R.-S. Huang, A. Wallraff, S. M. Girvin, and R. J. Schoelkopf, Phys. Rev. A **69**, 062320 (2004).

[32] N. J. S. Loft, M. Kjaergaard, L. B. Kristensen, C. K. Andersen, T. W. Larsen, S. Gustavsson, W. D. Oliver, and N. T. Zinner, "Quantum interference device for controlled two-qubit operations," (2019), arXiv:1809.09049.

[33] T. Toffoli, in *Automata, Languages and Programming*, edited by J. de Bakker and J. van Leeuwen (Springer, Berlin, 1980) pp. 632–644, lecture Notes in Computer Science Vol. 85.

[34] M. A. Nielsen and I. L. Chuang, *Quantum Computation and Quantum Information: 10th Anniversary Edition* (Cambridge University Press, 2010).

[35] L. Isenhower, M. Saffman, and K. Mølmer, Quantum Information Processing **10**, 755 (2011).

[36] K. Mølmer, L. Isenhower, and M. Saffman, Journal of Physics B: Atomic, Molecular and Optical Physics **44**, 184016 (2011).

[37] X.-F. Shi, Phys. Rev. Applied **9**, 051001 (2018).

[38] X. Wang, A. Sørensen, and K. Mølmer, Phys. Rev. Lett. **86**, 3907 (2001).

[39] S. E. Rasmussen, K. Groenland, R. Gerritsma, K. Schoutens, and N. T. Zinner, Phys. Rev. A **101**, 022308 (2020).

[40] E. Fredkin and T. Toffoli, International Journal of Theoretical Physics **21**, 219 (1982).

[41] S. E. Rasmussen and N. T. Zinner, "Simple implementation of high fidelity controlled-*i*swap gates and quantum circuit exponentiation of non-hermitian gates," (2020), arXiv:2002.11728.

[42] S. P. Pedersen, K. S. Christensen, and N. T. Zinner, Phys. Rev. Research **1**, 033123 (2019).

[43] T. Bækkegaard, L. B. Kristensen, N. J. S. Loft, C. K. Andersen, D. Petrosyan, and N. T. Zinner, Scientific Reports **9**, 13389 (2019).

[44] D. A. Meyer and N. R. Wallach, Journal of Mathematical Physics **43**, 4273 (2002).

[45] J. M. Lukens and P. Lougovski, Optica **4**, 8 (2017).

[46] H.-H. Lu, J. M. Lukens, N. A. Peters, O. D. Odele, D. E. Leaird, A. M. Weiner, and P. Lougovski, Phys. Rev. Lett. **120**, 030502 (2018).

[47] C. Reimer, S. Sciara, P. Roztocki, M. Islam, L. Romero Cortés, Y. Zhang, B. Fischer, S. Loranger, R. Kashyap, A. Cino, S. T. Chu, B. E. Little, D. J. Moss, L. Caspani, W. J. Munro, J. Azaña, M. Kues, and R. Morandotti, Nature Physics **15**, 148 (2019).

[48] M. Kues, C. Reimer, P. Roztocki, L. R. Cortés, S. Sciara, B. Wetzel, Y. Zhang, A. Cino, S. T. Chu, B. E. Little, D. J. Moss, L. Caspani, J. Azaña, and R. Morandotti, Nature **546**, 622 (2017).

[49] M. Kues, C. Reimer, J. M. Lukens, W. J. Munro, A. M. Weiner, D. J. Moss, and R. Morandotti, Nature Photonics **13**, 170 (2019).

[50] P. Imany, J. A. Jaramillo-Villegas, M. S. Alshaykh, J. M. Lukens, O. D. Odele, A. J. Moore, D. E. Leaird, M. Qi, and A. M. Weiner, npj Quantum Information **5**, 59 (2019).

[51] A. Monmayrant, S. Weber, and B. Chatel, Journal of Physics B: Atomic, Molecular and Optical Physics **43**, 103001 (2010).

[52] A. M. Weiner, Optics Communications **284**, 3669 (2011), special Issue on Optical Pulse Shaping, Arbitrary Waveform Generation, and Pulse Characterization.

[53] J. Capmany and C. Fernández-Pousa, Laser & Photonics Reviews **5**, 750.

Appendix A: Diamond gate

Here we present the Hamiltonian and unitary of the Diamond gate. For at more detailed discussion see [32]. The Hamiltonian of the diamond gate is

$$H = -\frac{1}{2}(\Omega+\Delta)(\sigma_z^{T1}+\sigma_z^{T2}) - \frac{1}{2}\Omega(\sigma_z^{C1}+\sigma_z^{C2}) + J_C\sigma_y^{C1}\sigma_y^{C2} + J(\sigma_y^{C1}+\sigma_y^{C2})(\sigma_y^{T1}+\sigma_y^{T2}). \tag{A1}$$

In the main text we set $J_C = 0$ and obtain the following unitary of the four qubit gate

$$U_{\text{dia}} = \begin{pmatrix}
1 & 0 & 0 & 0 & 0 & 0 & 0 & 0 & 0 & 0 & 0 & 0 & 0 & 0 & 0 & 0 \\
0 & 0 & -1 & 0 & 0 & 0 & 0 & 0 & 0 & 0 & 0 & 0 & 0 & 0 & 0 & 0 \\
0 & -1 & 0 & 0 & 0 & 0 & 0 & 0 & 0 & 0 & 0 & 0 & 0 & 0 & 0 & 0 \\
0 & 0 & 0 & -1 & 0 & 0 & 0 & 0 & 0 & 0 & 0 & 0 & 0 & 0 & 0 & 0 \\
0 & 0 & 0 & 0 & 0 & 0 & 0 & 0 & -1 & 0 & 0 & 0 & 0 & 0 & 0 & 0 \\
0 & 0 & 0 & 0 & 0 & 1 & 0 & 0 & 0 & 0 & 0 & 0 & 0 & 0 & 0 & 0 \\
0 & 0 & 0 & 0 & 0 & 0 & 1 & 0 & 0 & 0 & 0 & 0 & 0 & 0 & 0 & 0 \\
0 & 0 & 0 & 0 & 0 & 0 & 0 & 0 & 0 & 0 & 0 & -1 & 0 & 0 & 0 & 0 \\
0 & 0 & 0 & 0 & -1 & 0 & 0 & 0 & 0 & 0 & 0 & 0 & 0 & 0 & 0 & 0 \\
0 & 0 & 0 & 0 & 0 & 0 & 0 & 0 & 0 & 1 & 0 & 0 & 0 & 0 & 0 & 0 \\
0 & 0 & 0 & 0 & 0 & 0 & 0 & 0 & 0 & 0 & 1 & 0 & 0 & 0 & 0 & 0 \\
0 & 0 & 0 & 0 & 0 & 0 & 0 & -1 & 0 & 0 & 0 & 0 & 0 & 0 & 0 & 0 \\
0 & 0 & 0 & 0 & 0 & 0 & 0 & 0 & 0 & 0 & 0 & 0 & -1 & 0 & 0 & 0 \\
0 & 0 & 0 & 0 & 0 & 0 & 0 & 0 & 0 & 0 & 0 & 0 & 0 & 0 & -1 & 0 \\
0 & 0 & 0 & 0 & 0 & 0 & 0 & 0 & 0 & 0 & 0 & 0 & 0 & -1 & 0 & 0 \\
0 & 0 & 0 & 0 & 0 & 0 & 0 & 0 & 0 & 0 & 0 & 0 & 0 & 0 & 0 & 1
\end{pmatrix}. \tag{A2}$$

Appendix B: Expressibility plots

Here we present expressibility plot for layers $L = 1, 2, 3$, and 4 for $N = 4, 6$, and 8 qubits.

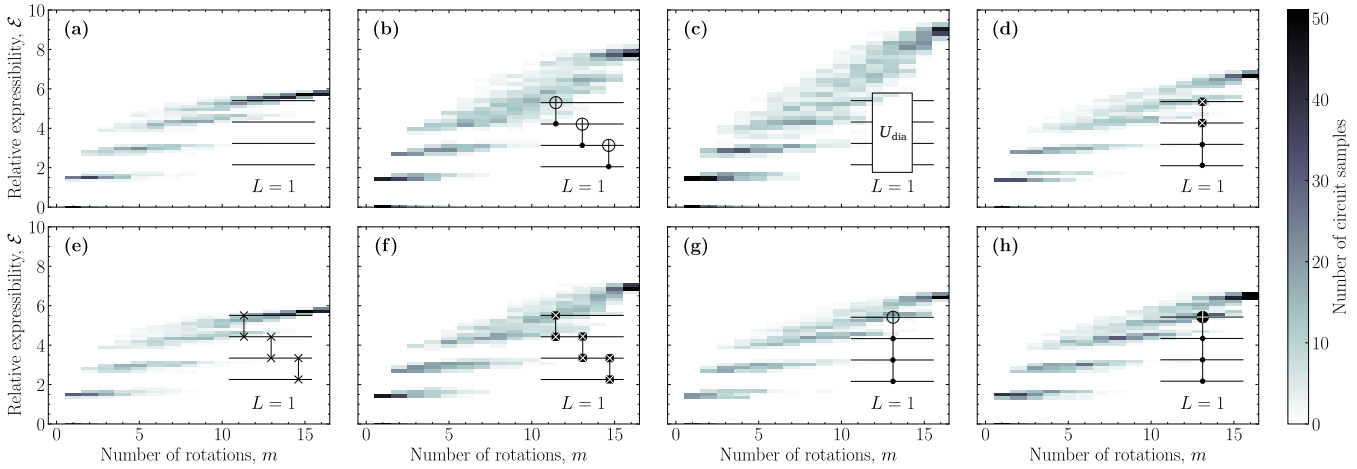


Figure 7. *Relative expressibility* of different circuits with $N = 4$ qubits and $L = 1$ layer as a function of the number of rotations. The inset in the right upper corner of each plot shows the entangling gate used in each layer. **(a)** Identity, **(b)** three CNOTs, **(c)** diamond gate, **(d)** double controlled *i*SWAP, **(e)** three SWAPs, **(f)** three *i*SWAPs, **(g)** triple controlled NOT, **(h)** triple controlled *i*NOT.

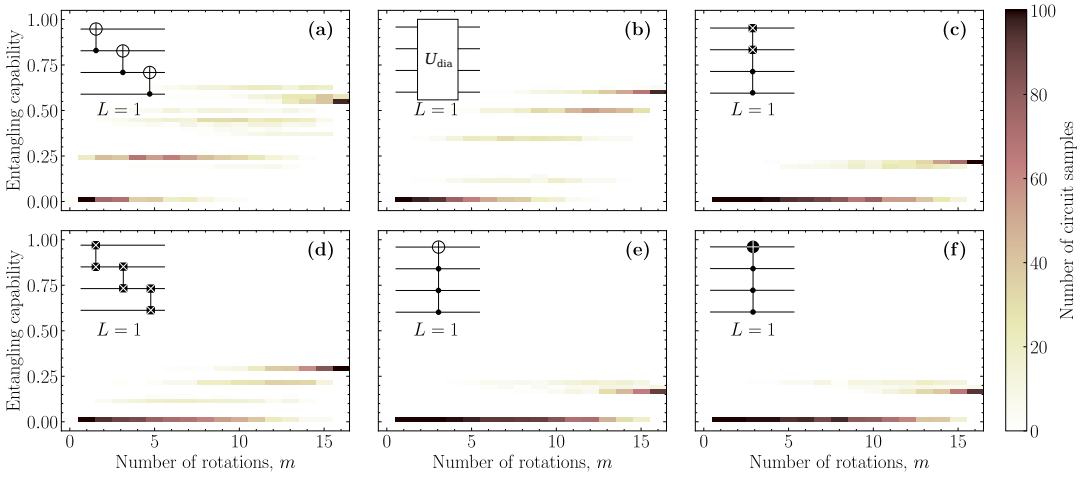


Figure 8. *Entangling capability* of different circuits with $N = 4$ qubits and $L = 1$ layer as a function of the number of rotations. The inset in the right upper corner of each plot shows the entangling gate used in each layer. **(a)** three CNOTs, **(b)** diamond gate, **(c)** double controlled *i*SWAP, **(d)** three *i*SWAPs, **(e)** triple controlled NOT, **(f)** triple controlled *i*NOT.

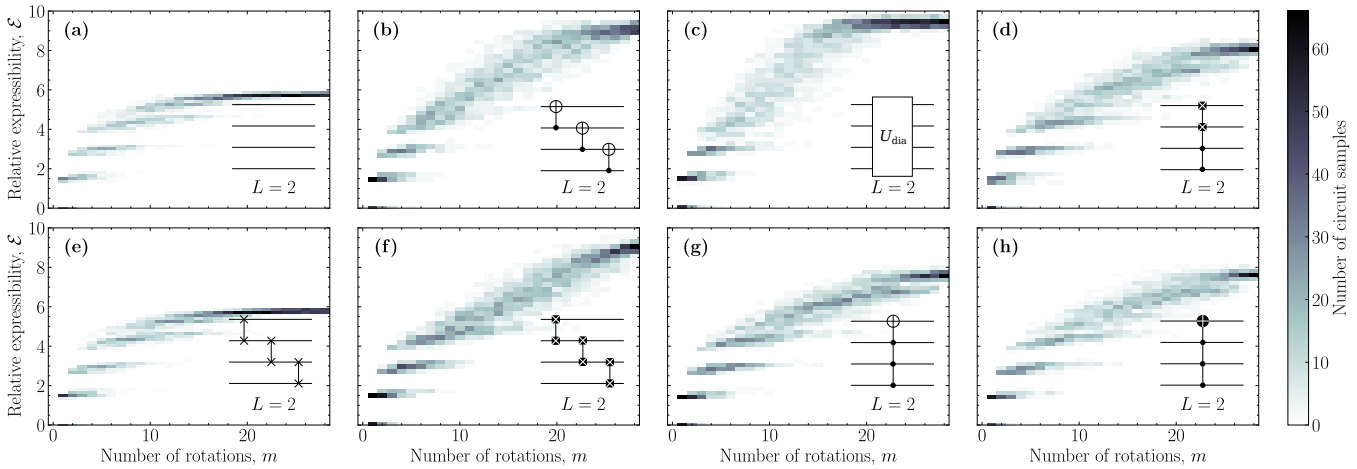


Figure 9. *Relative expressibility* of different circuits with $N = 4$ qubits and $L = 2$ layers as a function of the number of rotations. The inset in the right upper corner of each plot shows the entangling gate used in each layer. **(a)** Identity, **(b)** three CNOTs, **(c)** diamond gate, **(d)** double controlled *i*SWAP, **(e)** three SWAPs, **(f)** three *i*SWAPs, **(g)** triple controlled NOT, **(h)** triple controlled *i*NOT.

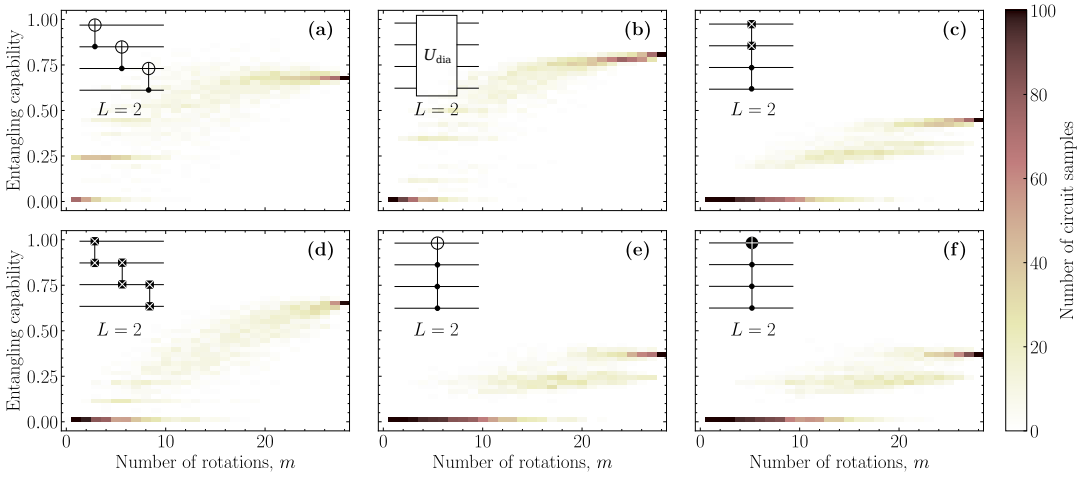


Figure 10. *Entangling capability* of different circuits with $N = 4$ qubits and $L = 2$ layers as a function of the number of rotations. The inset in the right upper corner of each plot shows the entangling gate used in each layer. **(a)** three CNOTs, **(b)** diamond gate, **(c)** double controlled *i*SWAP, **(d)** three *i*SWAPs, **(e)** triple controlled NOT, **(f)** triple controlled *i*NOT.

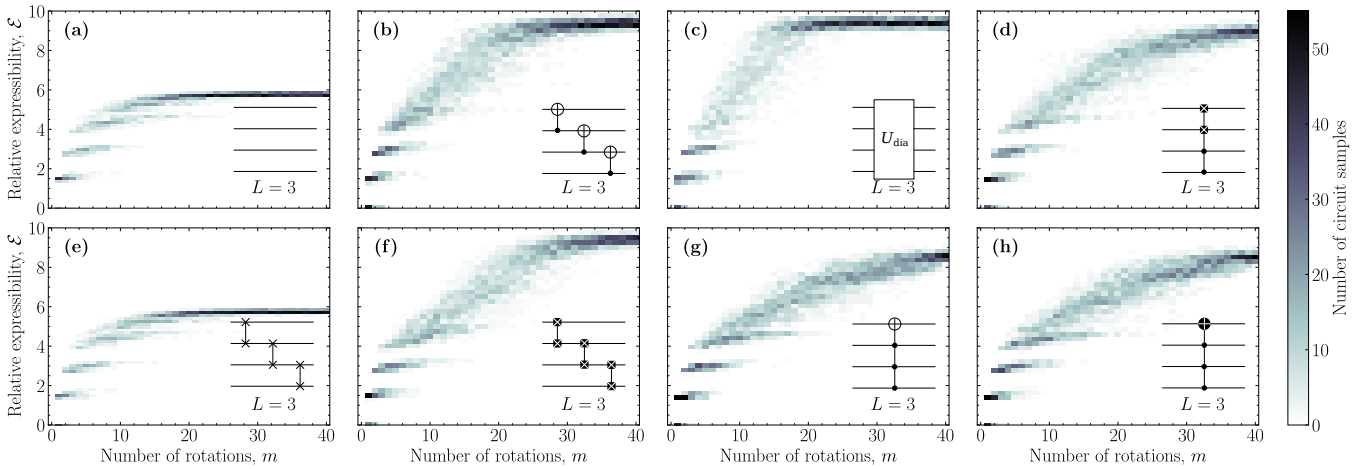


Figure 11. *Relative expressibility* of different circuits with $N = 4$ qubits and $L = 4$ layers as a function of the number of rotations. The inset in the right upper corner of each plot shows the entangling gate used in each layer. **(a)** Identity, **(b)** three CNOTs, **(c)** diamond gate, **(d)** double controlled *i*SWAP, **(e)** three SWAPs, **(f)** three *i*SWAPs, **(g)** triple controlled NOT, **(h)** triple controlled *i*NOT.

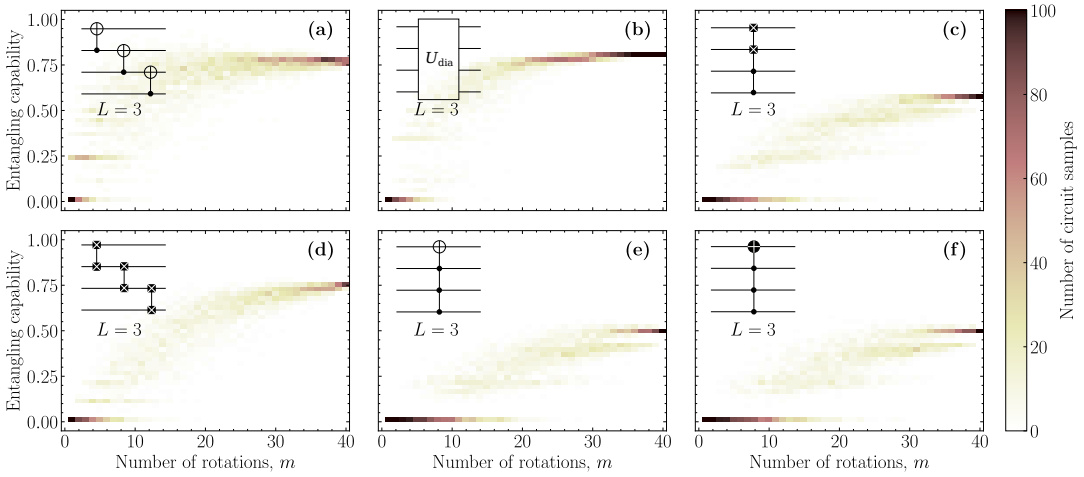


Figure 12. *Entangling capability* of different circuits with $N = 4$ qubits and $L = 4$ layers as a function of the number of rotations. The inset in the right upper corner of each plot shows the entangling gate used in each layer. **(a)** three CNOTs, **(b)** diamond gate, **(c)** double controlled *i*SWAP, **(d)** three *i*SWAPs, **(e)** triple controlled NOT, **(f)** triple controlled *i*NOT.

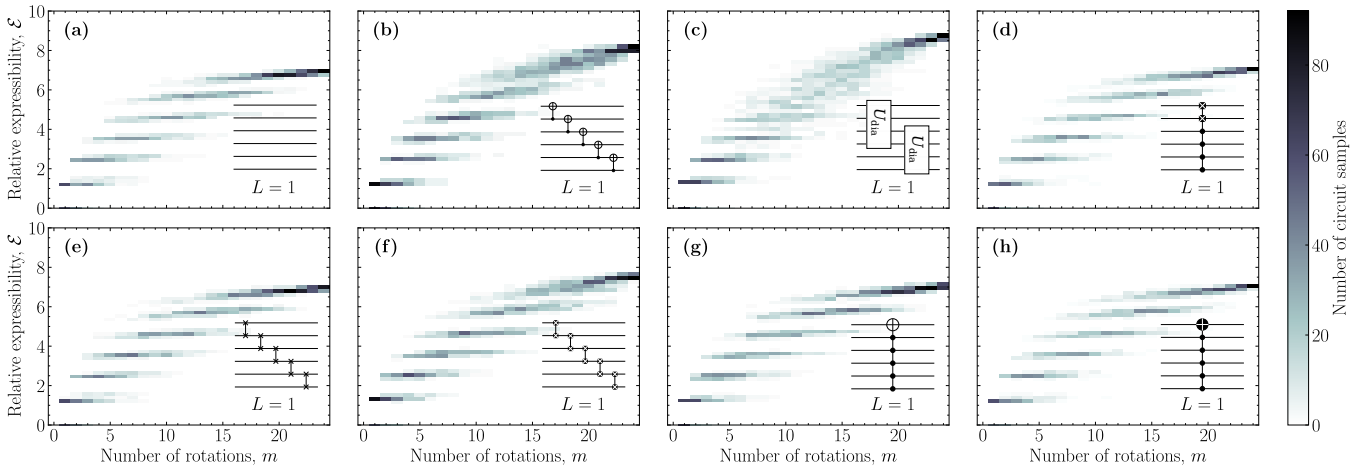


Figure 13. *Relative expressibility* of different circuits with $N = 6$ qubits and $L = 1$ layer as a function of the number of rotations. The inset in the right upper corner of each plot shows the entangling gate used in each layer. **(a)** Identity, **(b)** five CNOTs, **(c)** two diamond gates, **(d)** iSWAP with four control qubits, **(e)** five SWAPs, **(f)** five iSWAPs, **(g)** NOT with five control qubits, **(h)** iNOT with five control qubits.

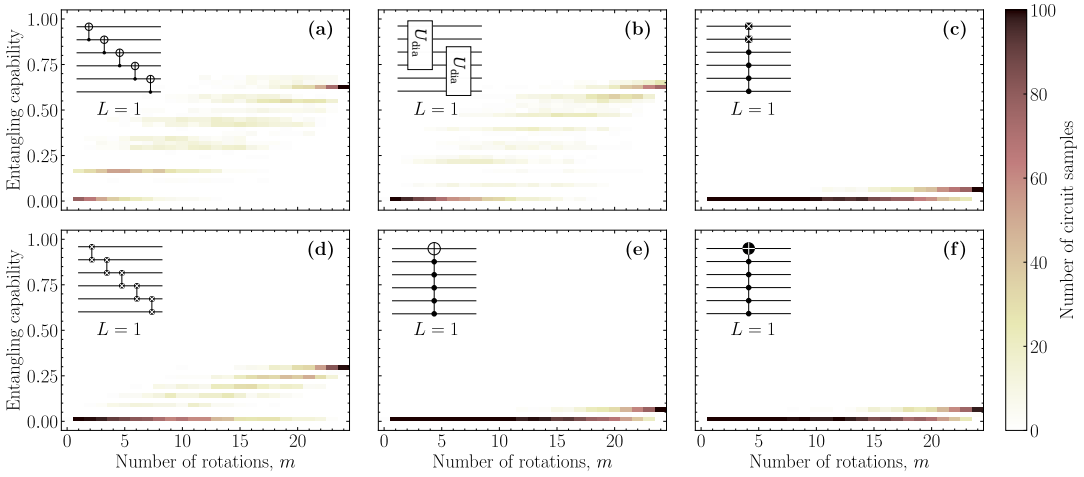


Figure 14. *Entangling capability* of different circuits with $N = 6$ qubits and $L = 1$ layer as a function of the number of rotations. The inset in the right upper corner of each plot shows the entangling gate used in each layer. **(a)** five CNOTs, **(b)** two diamond gates, **(c)** iSWAP with four control qubits, **(d)** five iSWAPs, **(e)** NOT with five control qubits, **(f)** iNOT with five control qubits.

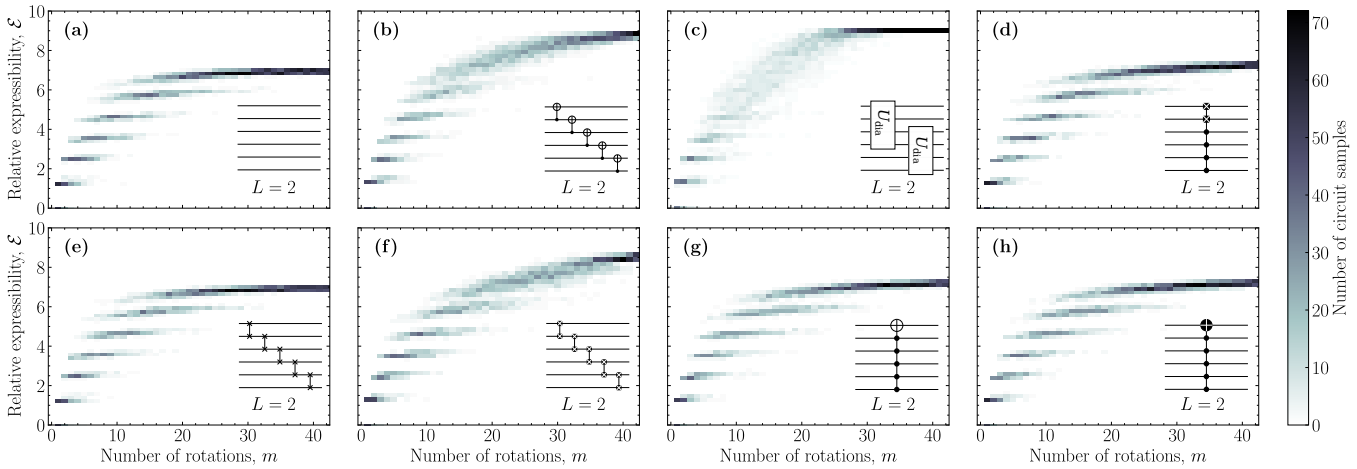


Figure 15. *Relative expressibility* of different circuits with $N = 6$ qubits and $L = 2$ layers as a function of the number of rotations. The inset in the right upper corner of each plot shows the entangling gate used in each layer. **(a)** Identity, **(b)** five CNOTs, **(c)** two diamond gates, **(d)** *i*SWAP with four control qubits, **(e)** five SWAPs, **(f)** five *i*SWAPs, **(g)** NOT with five control qubits, **(h)** *i*NOT with five control qubits.

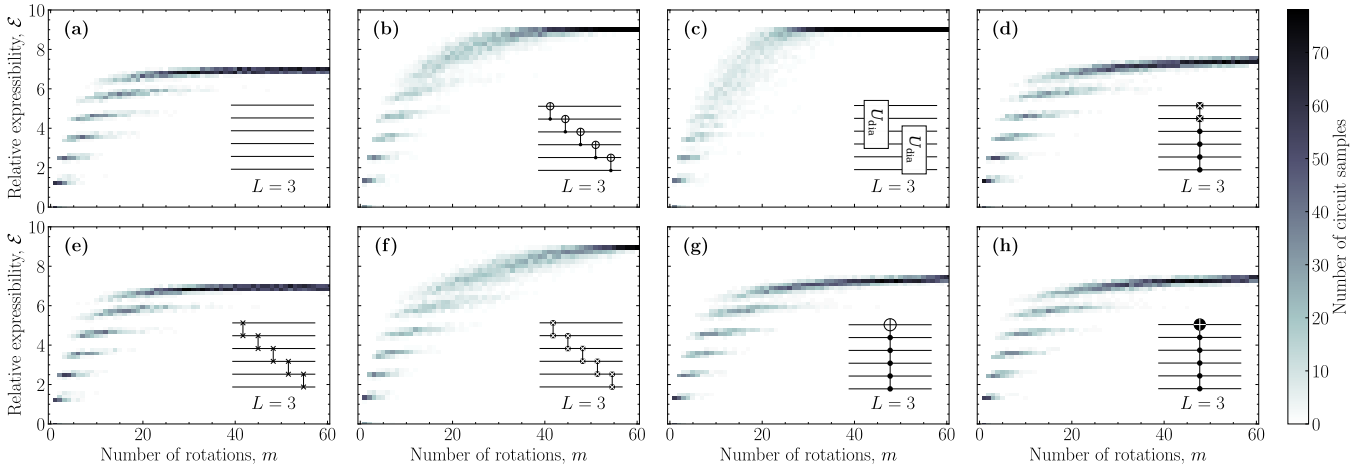


Figure 16. *Relative expressibility* of different circuits with $N = 6$ qubits and $L = 3$ layers as a function of the number of rotations. The inset in the right upper corner of each plot shows the entangling gate used in each layer. **(a)** Identity, **(b)** five CNOTs, **(c)** two diamond gates, **(d)** *i*SWAP with four control qubits, **(e)** five SWAPs, **(f)** five *i*SWAPs, **(g)** NOT with five control qubits, **(h)** *i*NOT with five control qubits.

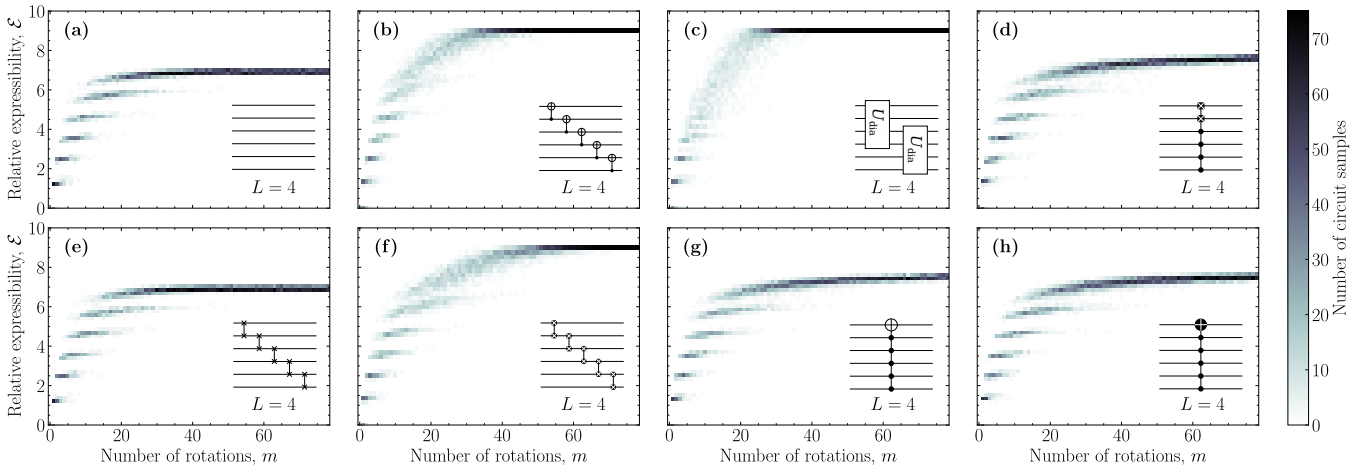


Figure 17. *Relative expressibility* of different circuits with $N = 6$ qubits and $L = 4$ layers as a function of the number of rotations. The inset in the right upper corner of each plot shows the entangling gate used in each layer. **(a)** Identity, **(b)** five CNOTs, **(c)** two diamond gates, **(d)** *i*SWAP with four control qubits, **(e)** five SWAPs, **(f)** five *i*SWAPs, **(g)** NOT with five control qubits, **(h)** *i*NOT with five control qubits.

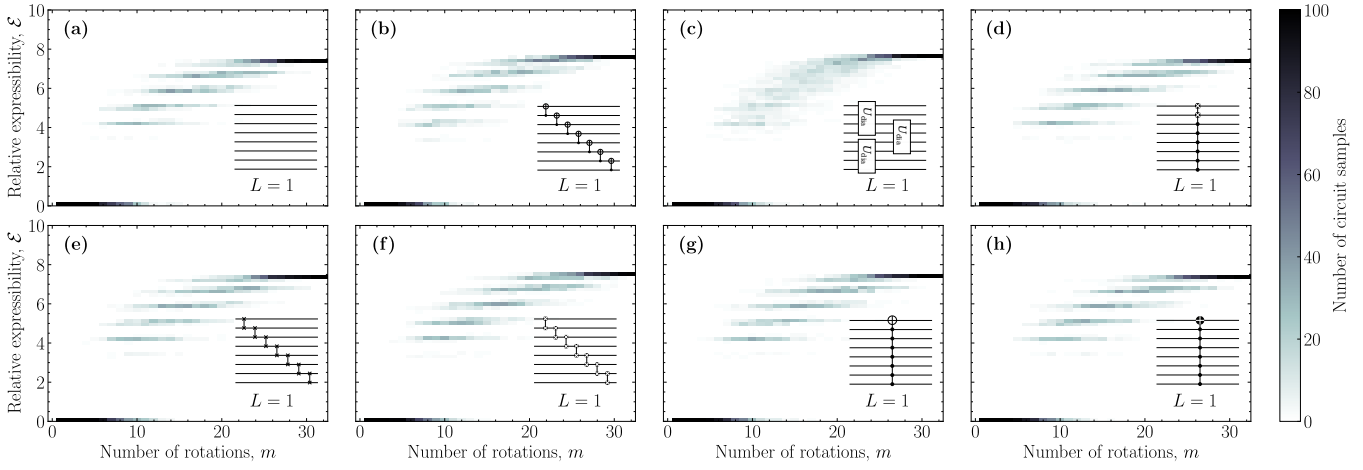


Figure 18. *Relative expressibility* of different circuits with $N = 8$ qubits and $L = 1$ layer as a function of the number of rotations. The inset in the right upper corner of each plot shows the entangling gate used in each layer. **(a)** Identity, **(b)** seven CNOTs, **(c)** three diamond gates, **(d)** *i*SWAP with six control qubit, **(e)** seven SWAPs, **(f)** seven *i*SWAPs, **(g)** NOT with seven control qubits, **(h)** *i*NOT with seven control qubits.

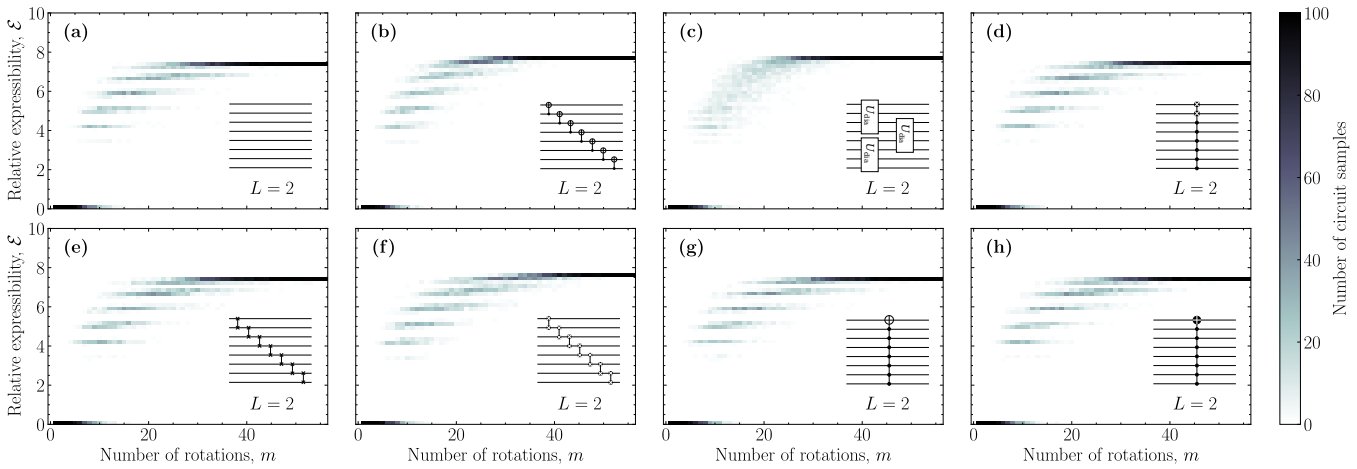


Figure 19. Relative expressibility of different circuits with $N = 8$ qubits and $L = 2$ layers as a function of the number of rotations. The inset in the right upper corner of each plot shows the entangling gate used in each layer. **(a)** Identity, **(b)** seven CNOTs, **(c)** three diamond gates, **(d)** iSWAP with six control qubit, **(e)** seven SWAPs, **(f)** seven iSWAPs, **(g)** NOT with seven control qubits, **(h)** iNOT with seven control qubits.

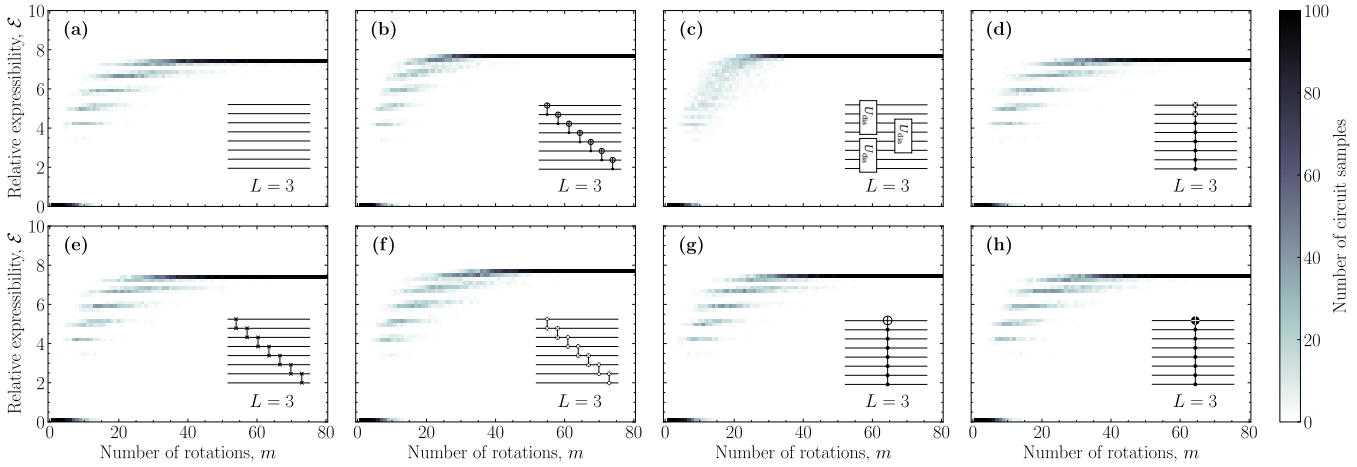


Figure 20. Relative expressibility of different circuits with $N = 8$ qubits and $L = 3$ layers as a function of the number of rotations. The inset in the right upper corner of each plot shows the entangling gate used in each layer. **(a)** Identity, **(b)** seven CNOTs, **(c)** three diamond gates, **(d)** iSWAP with six control qubit, **(e)** seven SWAPs, **(f)** seven iSWAPs, **(g)** NOT with seven control qubits, **(h)** iNOT with seven control qubits.

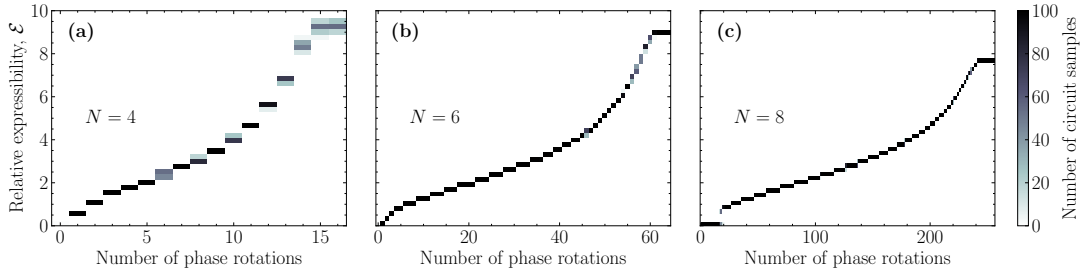


Figure 21. Relative expressibility of phase shaper gate corresponding to $N = 4, 6$, and 8 qubits and $L = 1$ layer as a function of the number of phase rotations.